BIOCHEMISTRY
including biophysical chemistry & molecular biology

Article

pubs.acs.org/biochemistry

# N-Terminal Disordered Domain of *Saccharomyces cerevisiae* Hop1 Protein Is Dispensable for DNA Binding, Bridging, and Synapsis of Double-Stranded DNA Molecules But Is Necessary for Spore Formation

Krishnendu Khan,[†] T. P. Vipin Madhavan,[†] Rucha Kshirsagar,[†] Kannan N. Boosi,[‡] Parag Sadhale,[‡,§] and K. Muniyappa*[,†]

[†]Department of Biochemistry, and [‡]Department of Microbiology and Cell Biology, Indian Institute of Science, Bangalore 560012, India

Supporting Information

**ABSTRACT:** The cytological architecture of the synaptonemal complex (SC), a meiosis-specific proteinaceous structure, is evolutionarily conserved among eukaryotes. However, little is known about the biochemical properties of SC components or the mechanisms underlying their roles in meiotic chromosome synapsis and recombination. Functional analysis of *Saccharomyces cerevisiae* Hop1, a key structural component of SC, has begun to reveal important insights into its function in interhomolog recombination. Previously, we showed that Hop1 is a structure-specific DNA-binding protein, exhibits higher binding affinity for the Holliday junction, and induces structural distortion at the core of the junction. Furthermore, Hop1 promotes DNA condensation and intra- and intermolecular synapsis between duplex DNA molecules. Here, we show that Hop1 possesses a modular domain organization, consisting of an intrinsically disordered N-terminal domain and a protease-resistant C-terminal domain (Hop1CTD). Furthermore, we found that Hop1CTD exhibits strong homotypic as well as heterotypic protein−protein interactions, and its biochemical activities were similar to those of the full-length Hop1 protein. However, Hop1CTD failed to complement the meiotic recombination defects of the Δ*hop1* strain, indicating that both N- and C-terminal domains of Hop1 are essential for meiosis and spore formation. Altogether, our findings reveal novel insights into the structure−function relationships of Hop1 and help to further our understanding of its role in meiotic chromosome synapsis and recombination.

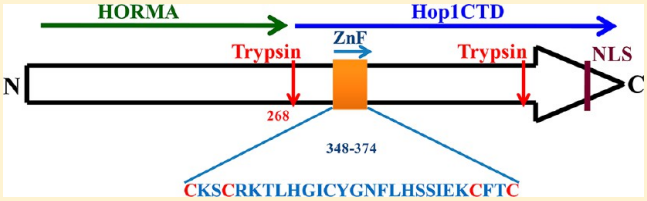


During meiosis I, reciprocal exchange between homologous chromosomes occurs in the context of a tripartite proteinaceous structure, the synaptonemal complex (SC).[1−4] The cytological architecture of SC, which is evolutionarily conserved from yeast to mammals, consists of two dense lateral elements (LEs) and a less dense central element; both are interconnected by numerous transverse elements.[2] Genetic evidence in a wide variety of organisms suggests that SC is also required for recombination intermediates to be converted to chiasmata and to ensure their disjunction and orderly segregation into gametes.[1−4] Our understanding of the basic processes underlying DSB formation and strand exchange has advanced substantially;[5−9] however, much less is known about the molecular mechanism by which the SC components help in various aspects of pairing between homologous chromosomes.

As meiotic prophase I progresses from leptotene through zygotene, the axial elements (AEs) become discernible; in pachytene the transverse filaments connect the AEs to form lateral elements along the entire length of homologues to generate a tripartite SC, which, in turn, ensures homologues become fully synapsed and the Holliday junctions (HJ) form.[6−9] Genetic analyses of meiosis in a number of organisms including *Saccharomyces cerevisiae* have revealed that a subset of mutants defective in meiotic chromosome pairing fail to make any detectable AE or SC structures.[2−4] In most organisms, DSB formation is necessary for recognition and pairing of homologues, whereas in some organisms these processes occur independently of DSB formation.[2,5,7] However, current evidence in yeast and mammalian cells demonstrate a strong correlation between the formation of programmed DSBs and the initiation of recombination.[5,7,9] Previous studies have suggested that SC plays a crucial role in the maturation of recombination intermediates during pachytene.[2,8,10−12] In *S. cerevisiae*, the genes that encode the structural components of axial/lateral and central elements include *HOP1*, *RED1*, *ZIP1*, *ZIP2*, and *ZIP3*.[13−19] The role that *HOP1* plays in the synapsis of homologous chromosomes has been studied in some detail by using a range of meiotic mutants.[20−26] Furthermore, Hop1 foci colocalize with Red1 foci to discrete sites on axial elements, consistent with the demonstration that a complex containing

**Received:** May 2, 2013
**Revised:** July 3, 2013
**Published:** July 10, 2013





dx.doi.org/10.1021/bi4005528 | *Biochemistry* 2013, 52, 5265−5279

Red1 and Hop1 is essential for synapsis.[24] Hop1 and Red1 proteins are the major structural components of LEs and are essential for homologous chromosome synapsis and chiasma formation.[14−16,25,26] However, only a handful of proteins have been characterized to date that are known to be involved in the formation of SC. For the few known SC-associated proteins, their functional specificity *in vitro* and the mechanistic consequences are unknown. By using Hop1 as a case study for proteins intrinsic to LEs, we previously showed that Hop1 is a structure-specific DNA-binding protein and exhibits higher binding affinity for the Holliday junction and G4 DNA.[27−31] Strikingly, Hop1 promotes DNA bridging, condensation, and intra- and intermolecular synapsis between duplex DNA molecules.[32] Altogether, these studies are consistent with the notion that Hop1 might play key roles at different stages of meiotic recombination.

The molecular mechanism(s) by which *S. cerevisiae HOP1* promotes synapsis of homologous chromosomes is not fully understood. Although the biochemical activities of Hop1 are relatively well understood, knowledge of protein structure and function relationships remains unclear. In this study, we have investigated the correlation between the Hop1 protein structure and its *in vitro* and *in vivo* functions including DNA binding, DNA synapsis, homotypic as well as heterotypic associations, and spore formation in meiosis. Our findings reveal that Hop1 has a modular organization consisting of a protease-resistant C-terminal domain that exhibits structure-specific DNA binding activity, DNA bridging, synapsis and condensation, and a protease sensitive intrinsically disordered N-terminus, and both are critical for meiotic recombination and spore formation.

## MATERIALS AND METHODS

**Bacterial Strains, Enzymes, and Biochemicals.** Fine chemicals were purchased from GE Biosciences or Sigma Chemical Company. Restriction endonucleases, T4 DNA ligase, T4 polynucleotide kinase, and Taq polymerase were purchased from New England Biolabs. *Escherichia coli* strain BL-21 star (DE3) and plasmid pET21a and pET28a were purchased from InVitrogen or Stratagene. Fast performance liquid chromatography columns were purchased from GE Biosciences. [$\gamma$-$^{32}$P]ATP was purchased from Bhabha Atomic Research Centre, Mumbai.

**Construction of DNA Substrates.** Synthetic oligonucleotides (ODNs) were purchased from Sigma-Genosys, and their sequences are shown in Supplementary Table S1, Supporting Information. ODNs were labeled at the 5′-end by using [$\gamma$-$^{32}$P]ATP and T4 polynucleotide kinase. The HJ, duplex, and the ssDNA substrates were prepared and characterized as previously described.[31] Briefly, stoichiometric amounts of four ODNs were annealed by incubation in 0.3 M sodium citrate buffer (100 $\mu$L), pH 7, containing 0.3 M NaCl at 95 °C for 3 min, followed by slow cooling at 20 °C. The HJ was prepared by mixing ODN1, ODN2, ODN3, and ODN4, and double-stranded DNA with ODN1 and ODN5. The annealed mixture was subjected to electrophoresis through a 6% polyacrylamide gel in 45 mM Tris-borate buffer (pH 8.3) containing 1 mM EDTA at 10 V/cm for 3 h. The bands corresponding to the annealed DNA products were excised from the gel and eluted in TE buffer (10 mM Tris-HCl, pH 7.5, 1 mM EDTA). The identity of DNA substrates was confirmed by restriction digestion (data not shown). ODN6 was used to prepare G4 DNA in the presence of 120 mM KCl by heating it up to 95 °C for 5 min followed by overnight cooling. The mixture was electrophoresed on a 8% polyacrylamide gel in 45 mM Tris-borate buffer (pH 8.3) containing 1 mM EDTA and 120 mM KCl at 10 V/cm for 3 h. DNA was isolated from the gels as described above.

**Plasmid Construction and Tetrad Analysis.** The nucleotide sequences corresponding to the full-length Hop1 and Hop1CTD was amplified from pNH54-9 and cloned into the centromeric plasmid pRS416 under the control of *TEF* promoter as previously described.[33] The GFP version of the above constructs and the GFP only construct were also cloned in the same vector (Supplementary Table S2). The sequence corresponding to Hop1CTD was amplified and cloned in the pET21a vector. The clone was designated as pHop1CTD. The identity of recombinant constructs was ascertained by DNA sequencing. For tetrad analysis, *S. cerevisiae* strains used were derivatives of SK1 strain. *S. cerevisiae hop1*Δ DW10a mutant strain (kind gift from Nancy Hollingsworth) was transformed with vector bearing full-length Hop1 or Hop1CTD constructs. The transformants were first selected for growth on synthetic medium lacking uracil and further selected by repatching on the same plates. Cells were plated onto sporulation medium and incubated at 30 °C for 3−4 days. The asci were then selected individually and dissected, and the spores were allowed to grow on rich (YPD) medium.

**Limited Proteolysis of Hop1 Protein.** *S. cerevisiae* full-length Hop1 protein was purified as previously described.[29,34] Reaction mixtures (35 $\mu$L) contained 10 mM Tris-HCl (pH 7.5), 16 $\mu$g of Hop1, Hop1CTD or *Mycobacterium smegmatis* RecA, $ZnCl_2$ (where specified), 5−50 nM HJ or duplex DNA (where specified) and trypsin or chymotrypsin at the indicated concentrations. After incubation at 4 °C for 10 min, reaction was terminated by the addition of 8 $\mu$L of SDS-PAGE sample buffer and PMSF to a final concentration of 0.2 mM. Samples were incubated at 95 °C for 5 min. Aliquots of denatured samples were separated through a 10% SDS-polyacrylamide gel. The gels were stained and visualized with silver nitrate. Following protease digestion, peptide fragments were separated by SDS-PAGE, transferred to PVDF membrane sheets, and visualized by Ponceau S staining. Individual bands were then excised from the PVDF membrane sheets and subjected to N-terminal sequencing by automated Edman degradation using a 477A protein sequencer (Applied Biosystems).

**Overexpression and Purification of Hop1CTD.** A single colony of *E. coli* cells bearing the plasmid pHop1CTD was inoculated into LB broth (3 L) supplemented with 100 $\mu$g/mL ampicillin and 34 $\mu$g/mL chloramphenicol. Cells were grown with vigorous shaking at 37 °C, until the cell density at $A_{600}$ nm reached 0.5. Hop1CTD expression was induced with the addition of IPTG to a final concentration of 0.5 mM and incubated further for an additional 12 h at 18 °C. Cells were collected by centrifugation, washed in STE buffer [10 mM Tris-HCl (pH 8), 100 mM NaCl and 1 mM EDTA], resuspended in buffer A [20 mM Tris-HCl (pH 6.8), 5 mM 2-mercaptoethanol, 50 mM NaCl, 10% (v/v) glycerol, 1 $\mu$g/mL each of aprotinin, pepstatin, leupeptin and 1 mM benzamidine], and stored at −80 °C. Cells were thawed and lysed by sonication (model no. GEX-750, ultrasonic processor) on ice at 60% duty cycles in a pulse mode. The sonicated suspension was centrifuged in a Beckman Ti-45 rotor at 30 000 rpm for 1 h at 4 °C. The supernatant was loaded onto a 10 mL SP Sepharose Fast Flow (SIGMA) column, which had been pre-equilibrated with buffer A. After the column was washed with 50 mL buffer A, the bound proteins were eluted with a linear gradient of NaCl (100


dx.doi.org/10.1021/bi4005528 | *Biochemistry* 2013, 52, 5265−5279

mM → 500 mM) in buffer A. The fractions containing Hop1CTD were pooled and dialyzed against buffer B (20 mM Tris-HCl, pH 7.5, 500 mM NaCl, 10% glycerol and 5 mM 2-mercaptoethanol) to equilibrate the protein pool with the column buffer. The dialysate was loaded onto a Superdex 200 column (120 mL), which had been pre-equilibrated with buffer B. The peak fractions containing Hop1CTD were pooled and dialyzed against buffer C (20 mM Tris-HCl, pH 7.5, 50 mM NaCl, 10% glycerol and 1 mM DTT). The dialysate was loaded onto a double-stranded DNA cellulose column (10 mL) pre-equilibrated with buffer C. After the column was washed with 50 mL of buffer C, the bound proteins were eluted with a linear gradient of NaCl (100 mM → 500 mM) in buffer C. The fractions containing Hop1CTD were pooled and dialyzed against storage buffer (20 mM Tris-HCl, pH 7.5, 200 mM NaCl, 20% glycerol and 1 mM DTT). The concentration of Hop1CTD was determined by dye-binding method using BSA as a standard. Purified Hop1CTD was free of exo- and endonucleases (data not shown). Aliquots of Hop1CTD in dialysis buffer were stored in −80 °C. The yield varied between 2 and 2.5 mg/g of cell paste.

**Electrophoretic Mobility Shift Assays.** Assays were performed as previously described.[31] Reaction mixtures (20 μL) contained 20 mM Tris-HCl (pH 7.5), 0.1 mM $ZnCl_2$, 1 nM 5′ $^{32}$P-labeled DNA, 150 mM NaCl and increasing concentrations of Hop1CTD. After incubation at 30 °C for 30 min, 2.5 μL of 10× gel loading buffer [0.42% (w/v) bromophenol blue and xylene cyanol in 50% glycerol] was added to each sample, and they were electrophoresed through a 8% native polyacrylamide gel in 45 mM Tris-borate buffer (pH 8.3) containing 1 mM EDTA at 10 V/cm for 3−6 h at 4 °C. The dried gel was exposed to phosphorimager screen, and the signals were visualized using a Fuji phosphorimager (FLA 9000).

**Chemical Cross-linking of Hop1CTD.** Assays were performed as previously described.[29] Briefly, reaction mixtures (20 μL) contained 10 mM Tris-HCl (pH 7.5), 10% glycerol, 50 mM NaCl, 10 μM Hop1CTD and the indicated amounts of freshly diluted glutaraldehyde. After incubation at 25 °C for 30 min, samples were diluted into gel loading buffer, and incubation was extended at 95 °C for 5 min. Reaction mixtures were separated through a 10% SDS-polyacrylamide gel and visualized by staining with silver nitrate.

To validate the results obtained from glutaraldehyde cross-linking, we used 4,4′-diisothiocyanatostilbene-2,2′disulfonic acid (DIDS). Reaction mixtures (20 μL) contained 10 mM Tris-HCl (pH 7.5), 50 mM NaCl, 10 μM Hop1CTD and the indicated amounts of freshly diluted DIDS. After incubation at 37 °C for 3 h, samples were diluted into gel loading buffer, and incubation was extended at 95 °C for 5 min. Samples were separated through a 10% SDS-polyacrylamide gel and visualized by staining with silver nitrate.

**Atomic Force Microscopy.** AFM experiments were performed as previously described.[32] Plasmid pNB10 and pET21a DNA was isolated from cultures of *E. coli* DH5α strain using the Qiagen maxiprep kit and resuspended in water. Linear DNA was prepared by digestion of pET21a closed circular DNA with *Eco*RI, followed by isolation from the gel using the Qiagen gel extraction kit. Hop1CTD (200 nM) and 5 ng of DNA were incubated in a reaction buffer (10 μL) containing 20 mM Tris-HCl (pH7.5), 0.1 mM $ZnCl_2$, and 2 mM $MgCl_2$. After 30 min incubation, 5 μL aliquots of the samples were applied to the surface of freshly cleaved mica. Images were acquired in air using a SNL (silicon-tip on nitride lever) AFM probe (Agilent Technologies, Force constant 21−98 N/m) and Agilent AFM controller operated in tapping mode. Imaging was done at a resolution of 512 × 512 pixels. Raw data were selected with the Picoimage software, and the same was used to "flatten" AFM images with second-order polynomial fitting.

**Dynamic Light Scattering.** Dynamic light scattering (DLS) experiments were performed using a Dynapro light scattering instrument (Wyatt Technology Compnay). The hydrodynamic radius ($R_H$) of a protein macromolecule in solution is calculated by the intensity of light scattered by it. Purified Hop1 and Hop1CTD (1 mg/mL) were dialyzed against 20 mM HEPES-HCl (pH 7.5) buffer containing 200 mM NaCl and 5% glycerol (buffer filtered through a 0.45 μm pore size filter) and centrifuged at 18 000 rpm (42200*g*) at 4 °C for 30 min. Several measurements were performed at 25 °C and analyzed using DYNAMICS ver.3.30 software (Protein Solutions). Data collection times of 10 s were used in all the cases, for a minimum of 20 acquisitions.

**Circular Dichroism Spectroscopy.** Far-UV circular dichroism (CD) spectra were recorded using a Jasco-815 spectropolarimeter equipped with a Peltier stage (Japan Spectroscopic Co., Japan) at 25 °C. Typically, the spectra were recorded from 190 to 260 nm with 20 mdeg sensitivity at a scan speed of 50 nm using 1 mg/mL protein in a 2 mm path length cuvette with a bandwidth of 2 nm. Each spectrum is an average of at least three scans. The spectra were corrected with the respective buffer control. The mean molar ellipticity values per residue were calculated using the software supplied by the manufacturer.

**Surface Plasmon Resonance Measurements.** All measurements were performed on a Biacore 2000 optical biosensor (GE Healthcare LifeScience). Protein immobilization, binding experiments, and data analysis were performed according to the templates supplied with the instrument's software. Briefly, Hop1 or Hop1CTD analyte was immobilized on the surface of a CM5 sensor chip (∼1000 response units (RU)/flow cell) using the amine coupling method. Unbound protein was removed by passing the buffer with a flow rate of 100 μL/min. One of the flow cells was treated with ethanolamine alone to serve as reference channel for non-specific binding. Binding experiments were carried out at 25 °C using a continuous flow of running buffer [10 mM HEPES buffer (pH 7.4) containing 150 mM NaCl, 50 mM EDTA and 0.005% P-20 surfactant] at a flow rate of 20 μL/min. Increasing concentrations of Hop1 or Hop1CTD were injected over CM5 sensor chip. The dissociation was followed for about 100 s in the same buffer. The surface was regenerated using the running buffer. The data obtained for the interaction between Hop1-Hop1, Hop1-Hop1CTD, and Hop1CTD-Hop1CTD were corrected for nonspecific binding by automatic subtraction of blank data from in-line reference flow cells. Data were analyzed using a 1:1 Langmuir binding model in BIAcore evaluation software 3.0 to determine the kinetic constants.

**Intrinsic and Extrinsic Fluorescence Measurements.** All the fluorescence measurements were made using a Jobin Yvon-Spex Fluoromax 3 fluorimeter (Instruments S. A., Inc.). For the intrinsic tryptophan fluorescence, excitation was done at 295 nm, and emission spectra were recorded in the range of 310−400 nm and corrected for the buffer blank. The excitation and emission slit widths were 2.5 and 2.5 nm, respectively. Reaction mixtures (180 μL) containing 20 mM Tris-HCl (pH 7.5), 0.1 mM $ZnCl_2$, and 1 μM full-length Hop1 or Hop1CTD

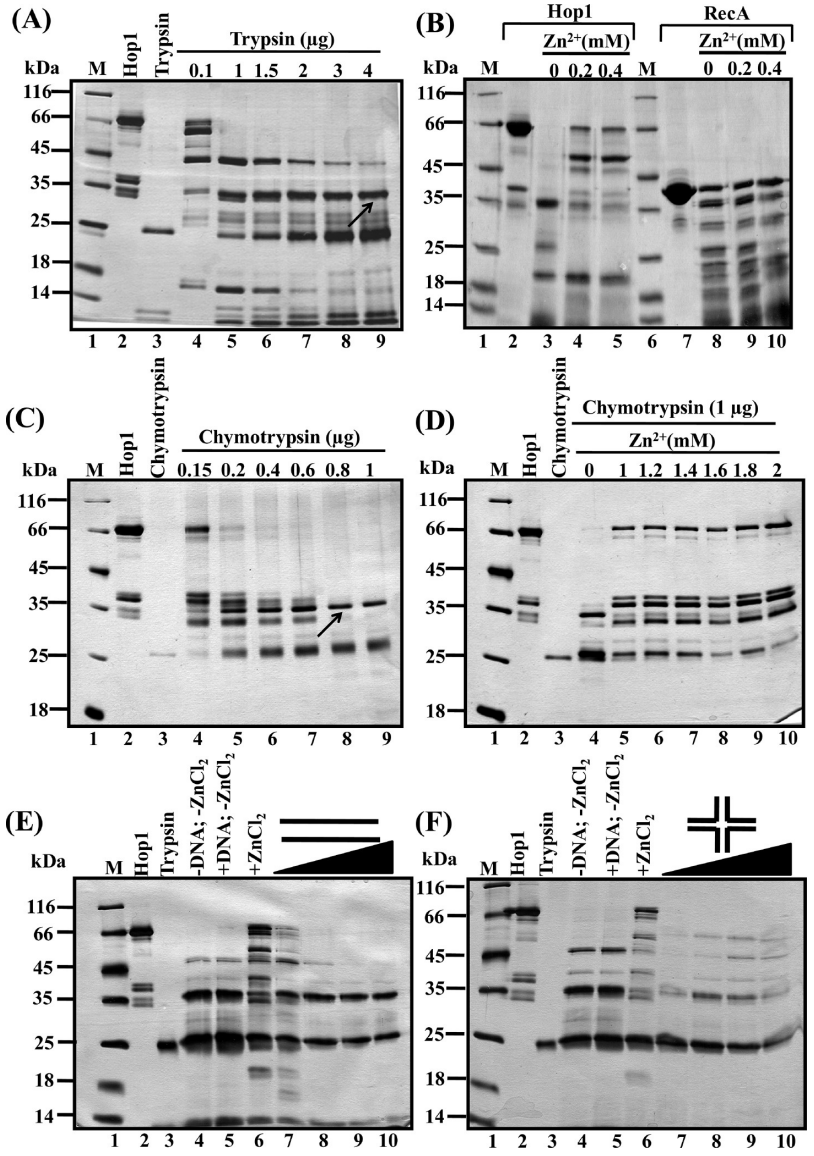


**Figure 1.** Limited proteolysis of Hop1 generates a protease-resistant C-terminal fragment. Trypsin and chymotrypsin digestions were performed at 4 °C for 10 min as described under Materials and Methods. (A) Proteolytic digestion of full-length Hop1 with increasing concentrations of trypsin; (B) $ZnCl_2$ confers partial protection to Hop1, but not to *M. smegmatis* RecA, against trypsin digestion; (C) Proteolytic sensitivity of full-length Hop1 to increasing concentrations of chymotrypsin; (D) $ZnCl_2$ confers partial protection to Hop1 against proteolytic cleavage; (E) Effect of double-stranded DNA and $ZnCl_2$ on digestion of Hop1 by trypsin; and (F) Effect of HJ and $ZnCl_2$ on digestion of Hop1 by trypsin. Panels A–F: Lane 1, standard protein markers; lane 2 shows full-length Hop1 and fragments generated by autocatalytic digestion. Panels A, C–F; lane 3 shows trypsin (2 $\mu$g) or chymotrypsin (1 $\mu$g). Panels B, D, E, and F: Hop1 was first incubated with increasing concentrations of $ZnCl_2$, double-stranded DNA, or HJ as indicated at 30 °C for 15 min, and then with trypsin or chymotrypsin at 4 °C for 10 min. Panels E and F: lanes 7–10 contained 5, 10, 25, and 50 nM of double-stranded DNA or HJ, respectively.

were incubated at 30 °C for 5 min. Quenching of intrinsic fluorescence by HJ was investigated as a function of its concentration, i.e., at 0.25, 0.5, 0.75, and 1 nM, respectively. The measurements were taken at 1 s intervals, and dilution was taken into account.

Reaction mixture (180 $\mu$L) used for the 1-anilino-8-naphthalene sulfonate (ANS) fluorescence measurements contained 20 mM Tris-HCl (pH 7.5), 0.1 mM $ZnCl_2$, 1 $\mu$M full-length Hop1, or Hop1CTD. Preliminary experiments were performed in order to determine the optimal concentration of ANS in the above buffer in the absence of DNA. After preincubation at 30 °C for 5 min, ANS was added to a final concentration of 20 $\mu$M. ANS binding and its fluorescence were measured at 30 °C with excitation at 390 nm, and emission spectra were recorded in the range of 400 and 600 nm, using bandwidths of 2.5 nm at 1 s intervals. Quenching of ANS fluorescence by HJ was investigated as a function of its concentration, i.e., at 0.25, 0.5, 0.75, and 1 nM, respectively. After incubation with HJ for 5 min, the spectra were recorded. The net fluorescence enhancement due to ANS binding to the protein was obtained by subtracting appropriate blank spectra of ANS in the buffer and corrected for inner filter effects.

**Subcellular Localization of GFP-Hop1 and GFP-Hop1CTD.** Exponentially growing *S. cervevisiae* Δ*hop1* DW10a strains containing pGFP, pGFPHop1, or pGFPHop1CTD were used for visualizing the subcellular location of the GFP fused proteins. Aliquots of mitotic cell cultures (2 mL) were centrifuged and washed three times with


dx.doi.org/10.1021/bi4005528 | *Biochemistry* 2013, 52, 5265–5279

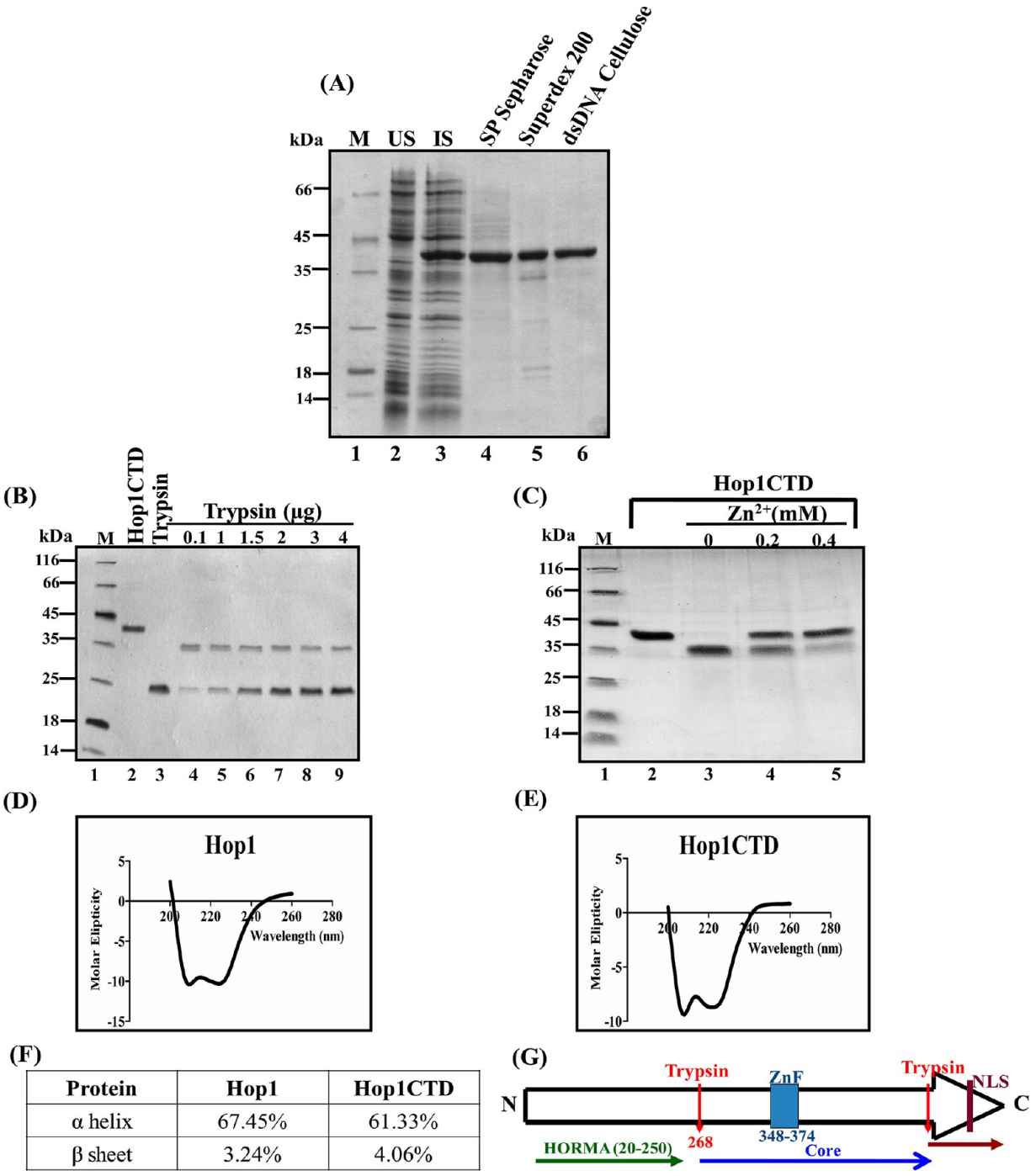


| Protein | Hop1 | Hop1CTD |
|---|---|---|
| α helix | 67.45% | 61.33% |
| β sheet | 3.24% | 4.06% |

**Figure 2.** Expression, purification, and CD analysis of Hop1CTD. (A) SDS-PAGE analysis showing induced expression Hop1CTD and at different stages of its purification. Lane 1, standard protein markers; lane 2, uninduced (US) cell-free lysate; lane 3, induced (IS) cell-free lysate; lane 4, chromatography on SP Sepharose; lane 5, chromatography on Superdex 200; lane 6, chromatography on double-stranded DNA cellulose. Twenty micrograms (lanes 2–3), 5 $\mu$g (lane 4), and 2 $\mu$g (lane 5 and 6) protein was resolved by SDS-PAGE and visualized by staining with Coomassie brilliant blue R-250. (B) Effect of increasing concentrations of trypsin on Hop1CTD. Lane 1, standard protein markers; lane 2, Hop1CTD; lane 3, trypsin (2 $\mu$g); lanes 4–6, Hop1CTD treated with the indicated concentrations of trypsin. (C) $ZnCl_2$ confers full protection to Hop1CTD against trypsin digestion. Lane 1, standard protein markers; lane 2, Hop1CTD in the absence of trypsin; lane 3, Hop1CTD in the absence of zinc and in the presence of trypsin; lane 4–5, Hop1CTD treated with trypsin in the presence of indicated amounts of zinc. (D) CD spectrum of full-length Hop1; (E) CD spectrum of Hop1CTD; (F) Secondary structural elements of Hop1 and Hop1CTD calculated from far-UV CD data. Far-UV CD spectra of Hop1 and Hop1CTD were recorded in 10 mM phosphate buffer (pH 7.5) at 25 °C in the spectral region of 190 to 260 nm and a scan speed of 50 nm/min. (G) Schematic showing the domain organization of full-length Hop1, derived from limited proteolysis experiments. NLS, nuclear localization signal.

1× PBS. Pelleted cells were resuspended in 70% ethanol and incubated at 4 °C. After 2 h, the cells were centrifuged, and the cell pellet was washed with 1× ice-cold PBS. Cell pellet was resuspended in 1 mL of 1× ice-cold PBS and sonicated (model no. GEX-750, Ultrasonic Processor) at 4 °C in a pulse mode, set at 21% duty cycles, for 10 s. After the addition of 100 $\mu$L of


dx.doi.org/10.1021/bi4005528 | *Biochemistry* 2013, 52, 5265–5279

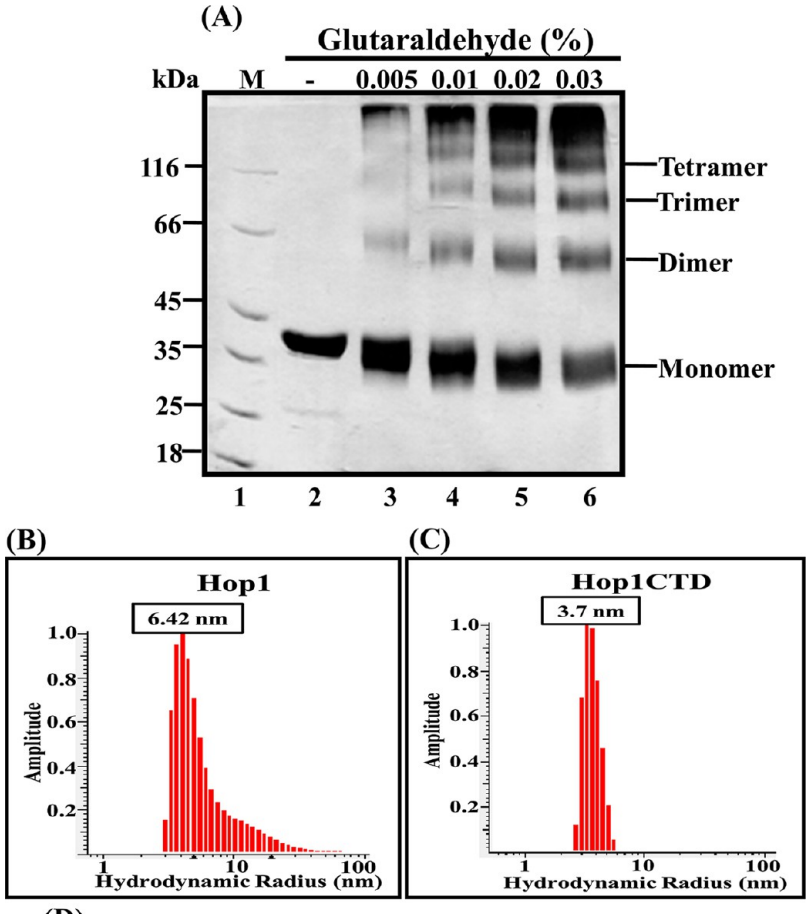


(D)

| Protein | Hydrodynamic radius (nm) | Monomeric Molecular weight (kDa) | Molecular weight from DLS (kDa) | Oligomeric state |
|---|---|---|---|---|
| Hop1 | 6.42 | 68.8 | 267.52 | Tetramer |
| Hop1CTD | 3.70 | 38 .2 | 72.75 | Dimer |

**Figure 3.** Oligomeric state of Hop1CTD. (A) Hop1CTD (10 $\mu$M) was incubated with increasing concentrations of glutaraldehyde as described under Materials and Methods. Lane 1 shows standard protein markers; lane 2 shows Hop1CTD incubated in buffer without glutaraldehyde; lanes 3–6, Hop1CTD incubated with increasing concentrations of glutaraldehyde as indicated. Reaction mixtures were analyzed by SDS-PAGE and visualized by silver staining. Positions of monomer, dimer, trimer, tetramer, and higher molecular species (in the wells) *are indicated* in the *right-hand side of the image*. (B) Dynamic light scattering analysis profile of full-length Hop1; (C) dynamic light scattering (DLS) analysis profile of Hop1CTD; (D) protein size distribution analysis obtained from DLS analysis. DYNAMICS v.3.3 software was used to determine the hydrodynamic radius.

RNase (stock 10 mg/mL), the cell suspension was incubated at 37 °C for 2 h in a shaker incubator. Propidium iodide (PI) was then added to a final concentration of 16 $\mu$g/mL, and cells were incubated at 4 °C for 7 h with continuous stirring. Cells were centrifuged, washed three times with 1× PBS, and resuspended in 200 $\mu$L of PBS. Aliquots of 10 $\mu$L were spotted onto sterile glass coverslips. The images of GFP, GFPHop1, or GFPHop1CTD and PI-stained nuclei were captured by fluorescence microscopy using Olympus B51 fluorescence microscope and were merged and further analyzed using adobe photoshop software.

## RESULTS

**Proteolytic Cleavage of Hop1 Generates a C-Terminal Fragment.** During the course of our studies, we observed that full-length Hop1 undergoes cleavage spontaneously by an autocatalytic mechanism when incubated at 4–37 °C (Supplementary Figure S1, Supporting Information). A number of different approaches, including N-terminal sequencing, FPLC, and MALDI-MS indicated that Hop1 preparation was free of any contaminating protease (data not shown). To investigate the domain organization of full-length Hop1, we subjected it to limited proteolysis with trypsin. The reaction products were analyzed by SDS-polyacrylamide gel electrophoresis and visualized by staining with silver nitrate. We observed that full-length Hop1 was fully digested, and as the concentration of trypsin was increased, the intermediate-sized fragments were further digested into smaller peptides (Figure 1A). Complete digestion of Hop1 resulted in two prominent fragments of ~45 kDa and ~35 kDa. Whereas the 45 kDa fragment was further digested with increase in trypsin concentration, the 35 kDa fragment was unusually resistant to digestion even at the highest concentration of trypsin used (Figure 1A, arrow). Previous work has shown that zinc binding


dx.doi.org/10.1021/bi4005528 | *Biochemistry* 2013, 52, 5265–5279

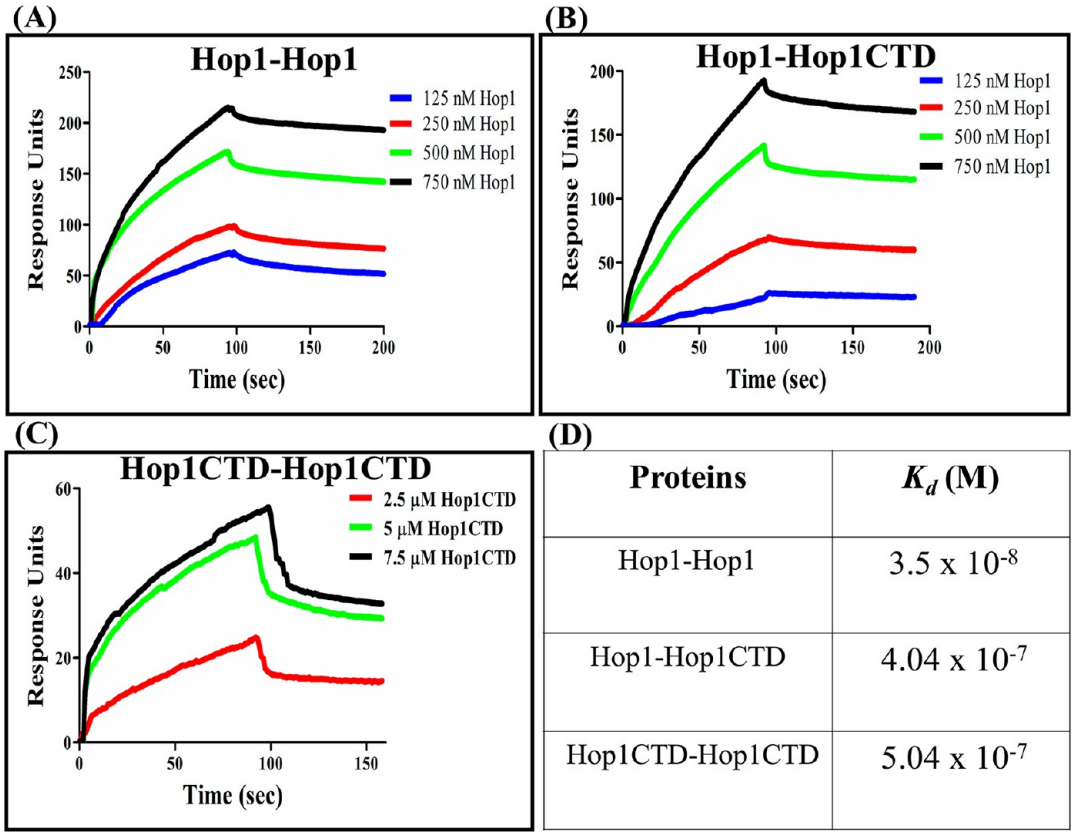


| Proteins | $K_d$ (M) |
|---|---|
| Hop1-Hop1 | $3.5 \times 10^{-8}$ |
| Hop1-Hop1CTD | $4.04 \times 10^{-7}$ |
| Hop1CTD-Hop1CTD | $5.04 \times 10^{-7}$ |

**Figure 4.** Surface plasmon resonance analysis of full-length Hop1 and Hop1CTD interactions. (A) Sensorgrams showing interaction of full-length Hop1 with increasing concentrations of full-length Hop1. (B) Sensorgrams showing interaction of Hop1CTD with increasing concentrations of full-length Hop1. (C) Sensorgrams showing interaction of Hop1CTD with increasing concentrations of Hop1CTD. The concentrations of soluble analytes are indicated in the inset to the figures. (D) Table shows the $K_d$ values determined using the 1:1 Langmuir model. Global fit of the data was used to calculate the binding constant. Data presented are representative of three independent experiments.

motif of Hop1 plays a crucial role in determining its DNA binding affinity.[29,32] To test its effect on the proteolytic sensitivity of Hop1, we incubated full-length Hop1 with a fixed amount of trypsin and increasing concentrations of $ZnCl_2$. Reaction mixtures were analyzed as described above. We observed that full-length Hop1 was partially digested, indicating that zinc provided protection to Hop1 against trypsin digestion (Figure 1B, compare lane 3 with lanes 4−5). To exclude the possibility that partial digestion was not due to inhibition of trypsin activity by zinc, we used *M. smegmatis* RecA as a control. Our results indicate that the proteolytic digestion pattern was very similar in the absence or presence of increasing concentrations of zinc, indicating that zinc at the concentrations used exerted no inhibitory effect on trypsin (Figure 1B, compare lane 8 with lanes 9−10).

To further explore the proteolytic sensitivity, Hop1 was incubated with increasing concentrations of chymotrypsin in the absence or presence of zinc. Aliquots of the incubation mixture were subjected to SDS-PAGE, and the reaction products were visualized as described above. As shown in Figure 1C, Hop1 was fully digested leading to the generation of 2−3 peptide fragments. However, the 35-kDa fragment was unusually resistant to chymotrypsin digestion, even at high protease concentrations. In similar experiments, but in the presence of increasing concentrations of $ZnCl_2$, Hop1 was partially digested yielding a distinctly different proteolytic footprint (Figure 1D). Additional experiments performed in the presence of DNA substrates also showed that Hop1 was cleaved to produce a major peptide of 35 kDa (Figure 1E,F). The 35 kDa band was excised and subjected to N-terminal amino acid sequencing. The N-terminal sequence (VDPFDLIL) obtained when aligned with the full-length Hop1 suggested that the cleavage site to be located at residue R268, thereby indicating that the 35 kDa fragment corresponds to the C-terminus of Hop1 protein. However, we note a significant difference between the theoretical (38 kDa) and observed molecular mass (35 kDa) of the C-terminus (see below). Thus, we conclude that the protease-resistant 35 kDa fragment represents the core domain of native Hop1 protein.

**Overexpression and Purification of Hop1 C-terminal Fragment.** The foregoing studies suggest that Hop1 undergoes spontaneous cleavage as well as is highly prone to proteolytic digestion. To characterize the protease-resistant Hop1 C-terminus (referred to hereafter as Hop1CTD), we designed a truncated construct of Hop1 encompassing the residues V269 to W605. Hop1CTD was expressed in and purified from BL21 star (DE3) strain of *E. coli* as described under Materials and Methods. Hop1CTD obtained from affinity chromatography on double-stranded DNA cellulose was homogeneous as judged by SDS-PAGE and had an apparent molecular weight of ∼38 kDa (Figure 2A).

**Limited Proteolysis of Hop1CTD.** We subjected Hop1CTD to limited proteolysis with trypsin in the absence or presence of $ZnCl_2$. Aliquots were analyzed by SDS-PAGE, followed by staining with silver nitrate. In the absence of $ZnCl_2$, Hop1CTD (38 kDa) was cleaved to form a 35 kDa fragment,


dx.doi.org/10.1021/bi4005528 | *Biochemistry* 2013, 52, 5265−5279

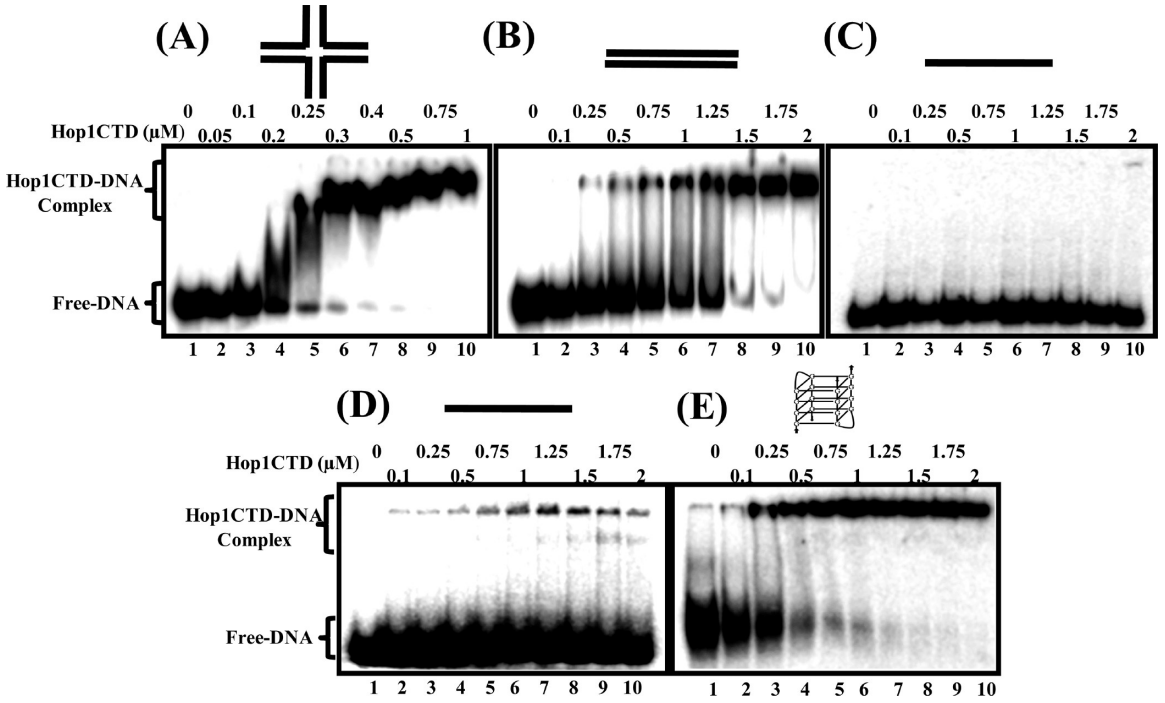


**Figure 5.** Hop1CTD binds non-B-DNA structures with high-affinity. (A) Hop1CTD binding to the Holliday junction. Assay was performed with 1 nM 5′ labeled HJ in the absence (lane 1) or presence of 50, 100, 200, 250, 300, 400, 500, 750, and 1000 nM Hop1CTD (lanes 2−10, respectively). (B) Binding of Hop1CTD to linear double-stranded DNA in the absence (lane 1) or presence of 100, 250, 500, 750, 1000, 1250, 1500, 1750, and 2000 nM (lanes 2−10, respectively). (C) Binding of Hop1CTD to ssDNA in the absence (lane1) or presence of 100, 250, 500, 750, 1000, 1250, 1500, 1750, and 2000 nM (lanes 2- 10, respectively). (D) Binding of Hop1CTD to ssDNA rich in G-residues in the absence (lane1) or presence of 100, 250, 500, 750, 1000, 1250, 1500, 1750, and 2000 nM (lanes 2−10, respectively). (E) Binding of Hop1CTD to G4 DNA in the absence (lane 1) or presence of 100, 250, 500, 750, 1000, 1250, 1500, 1750, and 2000 nM (lanes 2−10, respectively). The positions of free DNA and Hop1CTD-DNA complexes are indicated on the left-hand side of the images.

indicating the presence of a readily accessible site to trypsin (Figure 2B). On the other hand, in the presence of $ZnCl_2$, Hop1CTD was resistant to further digestion (Figure 2C). Analysis of cleavage products by MALDI-TOF mass spectrometry indicated that the trypsin cleavage site resides at R559. The resistance of 35 kDa fragment to further degradation indicates the presence of stable secondary structure which precludes protease access to the cleavage sites on Hop1. In accord, as shown in Figure 2D,E, the CD spectra of native Hop1 and Hop1CTD showed ellipticities at negative maxima between 220 and 222 nm and 207−209 nm, typical of that expected for a structured, predominantly $\alpha$-helical, protein.[35] The estimated secondary structure content ($\alpha$-helix and beta-strand) for Hop1CTD was comparable with that of the native Hop1 protein (Figure 2F). Figure 2G shows a schematic of the domain organization of full-length Hop1 and trypsin cleavage sites.

**Oligomeric State of Hop1 CTD.** Glutaraldehyde is a generalized cross-linking agent used extensively for the analysis of the oligomeric state(s) of proteins and has been previously used to study the oligomeric state of full-length Hop1.[29] Like full-length Hop1, incubation of Hop1CTD with glutaraldehyde resulted in the formation of dimer, trimer, tetramer, and higher oligomeric forms of increasing intensity (Figure 3A, lanes 3−6). Although Hop1CTD lacks a large N-terminal domain, it exerts no constraint on oligomerization. To validate direct interaction between Hop1CTD subunits and hence its oligomeric state in solution, we performed Hop1CTD cross-linking with DIDS, which has two equivalent isothiocyanate groups and cross-links between the two amino groups.[36] Like in the case of glutaraldehyde cross-linking, incubation with DIDS led to the formation of dimer, tetramer, and higher oligomeric forms of increasing intensity (Supplementary Figure S2).

To further ascertain the native molecular weight of Hop1CTD, we performed DLS measurements of both full-length Hop1 and Hop1CTD. The size distributions observed for Hop1 and Hop1CTD revealed particles of hydrodynamic radius ($R_H$) 6.42 and 3.7 nm, respectively (Figure 3B−D). These $R_H$ values indicate that full-length Hop1 oligomerized in a manner distinct from that of Hop1CTD. In particular, based upon a monomer weight of 68 kDa, the $R_H$ value for Hop1 suggested a tetrameric association assuming a globular protein, which is consistent with the data obtained from other studies,[29] while the $R_H$ value for Hop1CTD corresponds to 72 kDa, indicating that it exists primarily as a dimer in solution.

**Hop1 Exhibits Strong Homo- and Heterotypic Protein−Protein Interactions.** In view of the above, we examined the kinetics and binding affinities between Hop1 and Hop1CTD using surface plasmon resonance spectroscopy (SPR). Full-length Hop1 or Hop1CTD was immobilized on CM5 sensor chips, and varying concentrations of Hop1 or Hop1CTD were passed through a BIAcore flow cell. The sensograms were recorded for both homotypic (Hop1−Hop1 or Hop1CTD−Hop1CTD) and heterotypic (Hop1−Hop1CTD) association (Figure 4). At lower protein densities, we observed a measurable (but slow) off-rate but allowed calculation of dissociation kinetics. By comparison, at higher protein concentrations we observed distinct association and dissociation phases of binding, indicating that the kinetics of binding was rapid and that the binding reached equilibrium


dx.doi.org/10.1021/bi4005528 | Biochemistry 2013, 52, 5265−5279

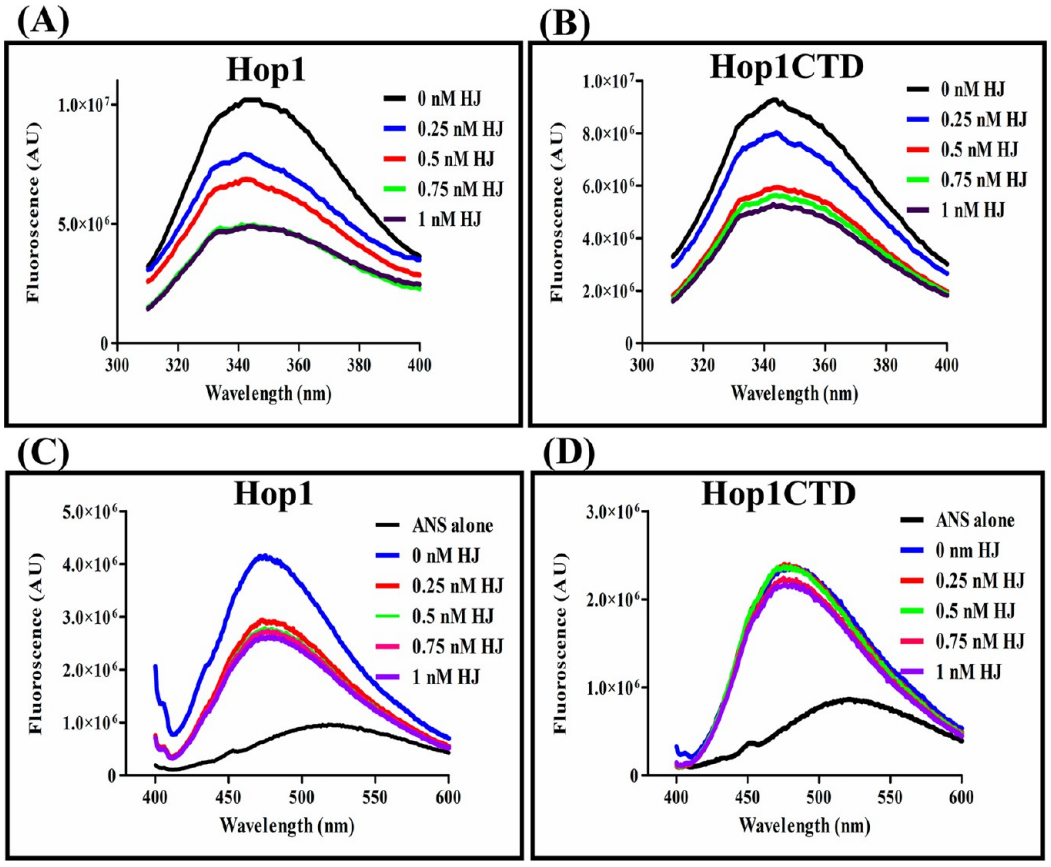


**Figure 6.** Quenching of intrinsic and extrinsic fluorescence of full-length Hop1 and Hop1CTD by the Holliday junction. (A) Changes in intrinsic tryptophan fluorescence of full-length Hop1 as a function of HJ concentrations. (B) Changes in intrinsic tryptophan fluorescence of Hop1CTD as a function of HJ concentrations. Samples were excited at 295 nm, and the emission spectra were recorded in the spectral region between 310 and 400 nm. (C) Changes in the full-length Hop1-ANS fluorescence as a function of HJ concentration. (D) Changes in the Hop1CTD-ANS fluorescence as a function of HJ concentration. The samples were excited at 390 nm, and the emission spectra were recorded in the spectral region between 400 and 600 nm. All the spectra shown are the average of three scans.

within ~100 s of the start of the injection, and dissociation was complete within ~20 s of the end of the injection. Analysis of sensorgrams, using a simple Langmuir model of 1:1 binding, revealed specific and concentration-dependent binding for all three combinations of associations; however, the association and dissociation profiles varied between each pair (compare Figure 4, panels A–B with panel C). The calculated dissociation rate constant ($k_d$) values from the SPR analyses are summarized in Figure 4D. The maximum response was obtained when Hop1 was injected over an immobilized Hop1 surface, while ~1-fold lower binding response was found for the homotypic or hetrotypic association between Hop1CTD and Hop1. Consistent with the chemical cross-linking data (Figure 3A), SPR assays indicate that Hop1 and Hop1CTD can form stable homo-oligomers with themselves and, more importantly, Hop1 and Hop1 CTD can also form hetero-oligomers.

**Hop1CTD Exhibits Higher Affinity for Non-B DNA Structures.** We next investigated the DNA substrate specificity of Hop1CTD using the electrophoretic mobility shift assay (EMSA). In this assay, the extent of binding was assessed by incubating varying concentrations of Hop1CTD with a fixed amount of HJ. As shown in Figure 5A, Hop1CTD was able to form a complex with the HJ, whose mobility gradually decreased with increasing protein concentrations and finally led to the formation of a well-defined higher-order complex. To examine the DNA binding specificity of Hop1CTD further, EMSA was performed with G4 DNA, double-stranded DNA (40 bp), and their constituent single strands. As shown in Figure 5B,E, incubation with a fixed amount of double-stranded or G4 DNA with increasing amounts of Hop1CTD resulted in the formation of a discrete protein–DNA complex. We note that Hop1CTD exhibited similar affinity to both HJ and G4 DNA, albeit in the $\mu$M range, but displayed relatively lower affinity for double-stranded DNA. Like full-length Hop1,[30] Hop1CTD was unable to bind to mixed-sequence 40-mer ssDNA or 49-mer ssDNA containing arrays of G-residues (Figure 5C,D). Thus, these results are consistent with the notion that Hop1CTD is the functional core of Hop1 protein.

**Quenching of Tryptophan Fluorescence of Hop1 and Hop1CTD by the Holliday Junction.** Secondary structure predictions indicated that a large part of the N-terminal domain of wild-type Hop1 is disordered, thus providing a reasonable explanation of why it readily undergoes spontaneous autocatalytic cleavage and is susceptible to proteolytic degradation (data not shown). To assess the conformational changes in the wild-type Hop1 and Hop1CTD, we first performed a series of titrations involving quenching of tryptophan fluorescence in the presence of increasing amounts of HJ. After excitation at 295 nm, we recorded the fluorescence emission spectra for full-length Hop1 (Figure 6A) and Hop1CTD (Figure 6B) at ~345 nm. The addition of increasing amounts of HJ to a reaction mixture containing a fixed amount


dx.doi.org/10.1021/bi4005528 | *Biochemistry* 2013, 52, 5265–5279

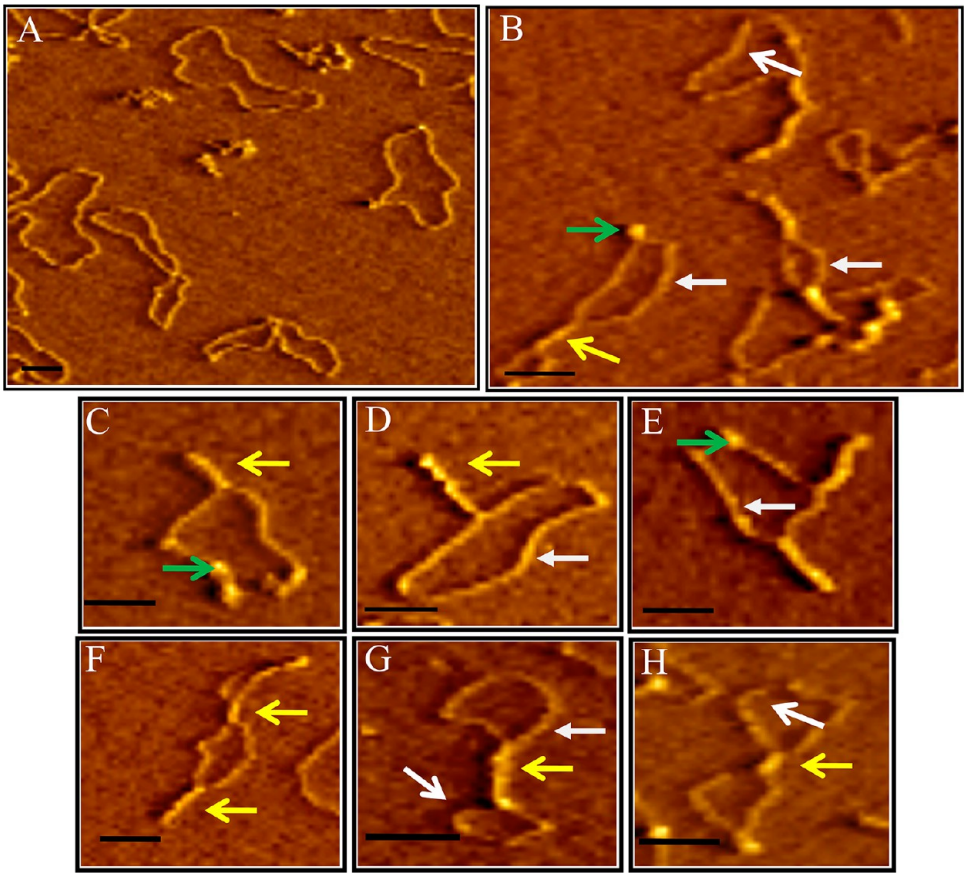


**Figure 7.** Hop1CTD promotes DNA bridging between noncontiguous DNA segments. (A) AFM images of closed circular duplex DNA in the absence of Hop1CTD and (B) after incubation with Hop1CTD. A 5 $\mu$L aliquot of the reaction mixture was spotted on fresh mica and visualized as described under Materials and Methods. Panels C–H illustrate randomly selected magnified images of Hop1CTD-DNA complexes. In the presence of Hop1, frequently observed structures include rigid rodlike structures due to bridging of DNA (yellow arrow), loop structures (white arrow), and higher-order nucleoprotein structures, which appear as globules to smaller rods (green arrow). The scale bars represent 200 nm (A and B) and 100 nm (C–F).

of wild-type Hop1 or Hop1CTD caused a commensurate decrease in the magnitude of fluorescence intensity of both the proteins, while the fluorescence emission spectra remained centered at 345 nm. Full-length Hop1 exhibited robust fluorescence quenching with increasing amounts of HJ, with saturation occurring between 0.5 and 0.75 nM (Figure 6A). On the other hand, although the fluorescence intensity profiles for Hop1CTD are reminiscent of wild-type Hop1, the magnitude of fluorescence quenching was less efficient and required a relatively higher concentration of HJ (~1 nM) to achieve a similar effect (Figure 6B).

**N-terminal Domain of Hop1 Is Intrinsically Disordered.** The fluorescence quantum yield of 8-anilino-1-naphthalenesulfonic acid (ANS) increases upon binding to hydrophobic sites of proteins, and this feature has been used extensively to study the structure and conformational changes in proteins.[37] We measured the extrinsic fluorescence of full-length Hop1 and Hop1CTD upon binding to ANS, in the absence or presence of HJ. Although ANS, by itself, exhibited low but measurable level of fluorescence, both Hop1 and Hop1CTD sharply enhanced the probe fluorescence and shifted its spectrum to the blue. In the presence of HJ, the magnitude of decrease in the fluorescence intensity was greater for full-length Hop1 than that observed for Hop1CTD (compare Figure 6C with 6D). Interestingly, even at higher concentration (1 nM), HJ had little or no significant effect on the fluorescence quantum yields of Hop1CTD. The absence of fluorescence spectral changes in Hop1CTD, compared to full-length Hop1, is consistent with the notion that while Hop1CTD retains the overall structure upon HJ binding full-length Hop1 does not.

**Hop1CTD Promotes DNA Bridging and Condensation.** To gain further insights into the mode of interaction of Hop1CTD with DNA, protein–DNA complexes were visualized using atomic force microscopy (AFM). We incubated Hop1CTD with circular duplex DNA and visualized under conditions similar to those used for full-length Hop1.[32] The representative AFM images shown in Figure 7 reveal different binding modes of Hop1CTD and the coexistence of structurally distinct Hop1CTD-DNA complexes (Figure 7B–H, as compared to naked DNA in Figure 7A). Binding of Hop1CTD to circular duplex DNA resulted in (i) the appearance of discrete "globules" (green arrows), (ii) bridging between two noncontiguous DNA segments to form single and double stem-loop structures (white arrows), and (iii) cooperative polymerization extends the bridges into rigid, rod-like nucleoprotein filaments (yellow arrows). The Hop1CTD-DNA complexes constituted >90% of observed molecules. DNA contour length measurements revealed a small reduction by ~1.5–2-fold, from 1200 nm ($n$ = 20) for naked DNA to 800–600 nm ($n$ = 25) after Hop1CTD binding, indicating DNA condensation. The experiments carried out for


dx.doi.org/10.1021/bi4005528 | *Biochemistry* 2013, 52, 5265–5279

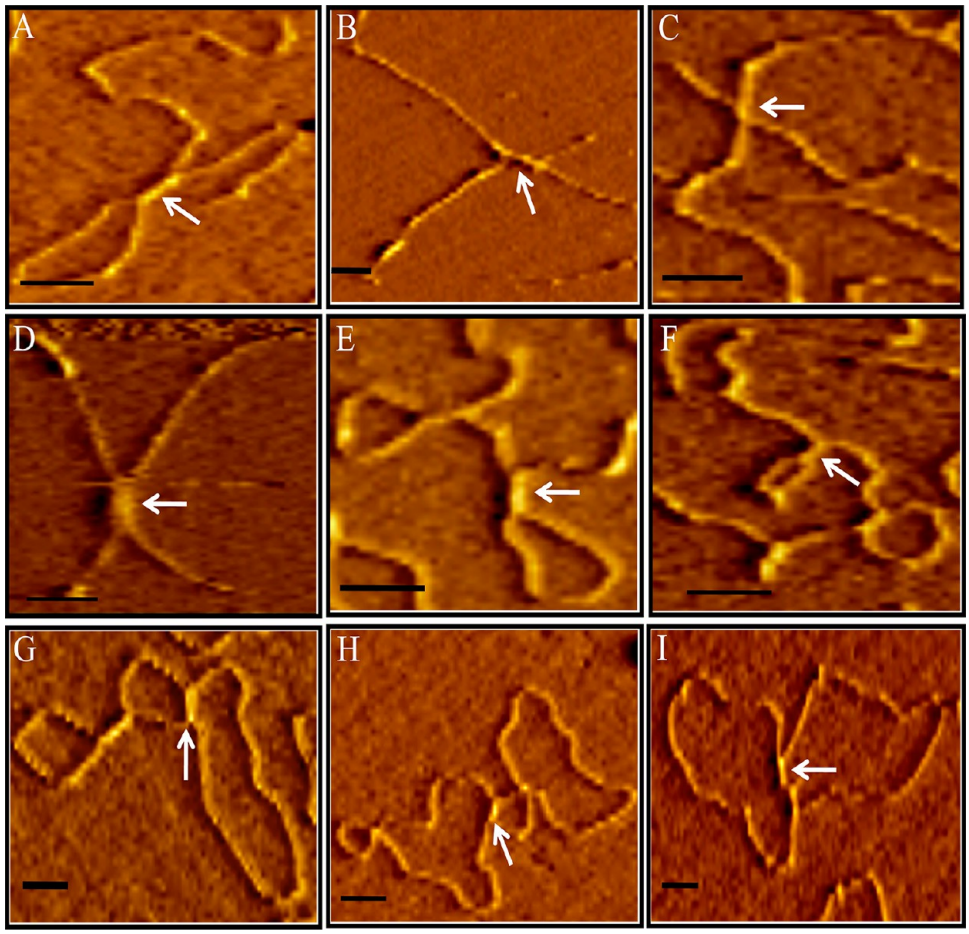


**Figure 8.** Hop1CTD promotes intra- and intermolecular synapsis between DNA molecules. Randomly selected AFM images showing inter- (panels A–D) and intramolecular (panels E, F) synapsis between linear duplex DNA molecules. Panels G–I depict AFM images showing intermolecular synapsis between circular DNA molecules. White arrows denote the site of intra- or intermolecular DNA synapsis. In all images, the scale bars indicate 100 nm.

different incubation times, ionic conditions, and concentrations of divalent cations yielded similar results (data not shown).

**Hop1CTD Promotes Intra- and Intermolecular Synapsis Between Linear or Circular DNA Molecules.** We further investigated the ability of Hop1CTD to promote synapsis between DNA molecules by using AFM. For this purpose, we kept Hop1CTD concentrations at low levels to overcome DNA bridging as well as the formation of DNA networks. Notably, we found that Hop1CTD was able to promote intermolecular synapsis wherein two linear duplex DNA molecules are bound in trans *in a typical* X-like synaptic configuration (Figure 8A–D). We also observed intramolecular synapsis at multiple sites (Figure 8E,F). Similarly, we found that Hop1CTD was able to promote both intra- and trans-synaptic structures between two closed circular DNA molecules, and stem-loop structures as a result of bridging between two noncontiguous segments of DNA (Figure 8). Altogether the results indicate that the formation of intra- and intermolecular synapsis is independent of sequence homology. The width measurements suggest that the DNA duplexes in the trans-synaptic structures are arranged in side-by-side orientation (Supplementary Figure S3).

**Hop1CTD Localizes to the Nucleus.** To examine the subcellular localization of Hop1CTD, we transformed *S. cerevisiae* strains that express the green fluorescent protein (GFP) fused translationally to the N-terminus of Hop1CTD and also GFP-encoding gene translationally fused to the N-terminus of wild-type Hop1-encoding gene (Supplementary Table S2). These recombinant expression constructs were introduced into exponentially growing *S. cerevisiae hop1*Δ strains. The transformants were selected on Ura$^-$ agar plates. Addition of GFP-encoding gene to *HOP1* or *hop1CTD*-encoding genes did not result in any apparent defect in vegetative growth and cell viability. Cells were fixed, stained with propidium iodide, and visualized under a fluorescence microscope. We found that GFP-Hop1 as well as GFP-Hop1CTD were expressed and concentrated in the nucleus as ascertained by staining of the nucleus with propidium iodide (Figure 9E–L). On the other hand, GFP alone was found fairly evenly distributed throughout the cell under these conditions (Figure 9A–D). In conclusion, these results indicate that Hop1CTD, which harbors a putative nuclear localization signal, allows its localization to the nucleus.

**Hop1CTD Failed To Complement the Meiotic Recombination Defects of *hop1*Δ Mutant.** To test the functional consequence of nuclear localization of Hop1CTD, we chose to complement the meiotic recombination defects of *hop1*Δ mutants. For this purpose, we constructed *hop1*Δ/*HOP1* and *hop1*Δ/*hop1CTD* strains, and the resulting strains were sporulated on solid medium at 30 °C and tested for the formation of viable spores by tetrad dissection. Table 1 shows spore viability data in SK1 isogenic strains, except for the


dx.doi.org/10.1021/bi4005528 | *Biochemistry* 2013, 52, 5265–5279

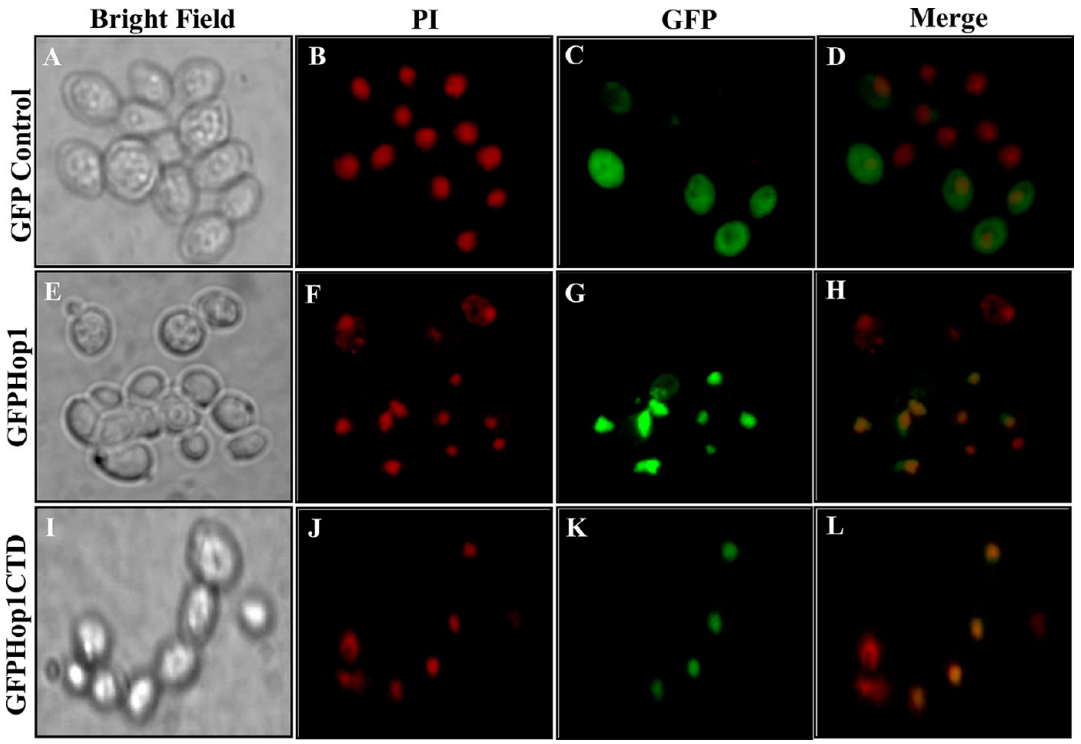


**Figure 9.** Hop1CTD localizes to the *S. cerevisiae* nucleus. The subcellular localization of full-length Hop1 and Hop1CTD was investigated using GFP fusion proteins. *S. cerevisiae hop1*Δ cells expressing different fusion proteins or GFP alone (control) were analyzed by fluorescence microscopy to detect GFP and/or propidium iodide signals as described under Materials and Methods. Bright field microscopy images taken in parallel were included as reference. (A–D) Expression analysis of GFP control. (E–H) Expression analysis of GFP-Hop1 fusion protein. (I–L) Expression analysis of GFP-Hop1CTD fusion protein. The merged images in panels D, H, and L show that both Hop1 and Hop1CTD are localized to the nucleus, whereas GFP was primarily localized in the cytoplasm.

**Table 1. Tetrad Analysis of *S. cerevisiae HOP1/HOP1*, *hop1*Δ*/hop1*Δ, *hop1*Δ*/HOP1*, and *hop1*Δ*/hop1*CTD Strains**[a]

| strain | no. of tetrads dissected | no. of spores | % spore viability |
|---|---|---|---|
| *HOP1/HOP1* | 28 | 112 | 96 |
| *hop1/hop1* | 26 | 104 | 0.96 |
| *hop1/HOP1* | 65 | 260 | 91.2 |
| *hop1/hop1*CTD | 26 | 104 | 0 |

[a]The indicated *S. cerevisiae* were analyzed for spore viability as described under Materials and Methods. The results show that *HOP1* is able to complement the *hop1*Δ strain, whereas *hop1*CTD fails to do so.

indicated mutations. Analysis of 26 tetrads derived from the *hop1*Δ*/hop1*Δ strain displayed ∼1% of the wild-type level of spore viability. The effect of *HOP1* complementation on the low spore viability was measured by the dissection and analysis of 65 tetrads from *hop1*Δ*/HOP1* strain. The data suggest that a single copy of *HOP1* was sufficient to restore the viability of the germinating spores nearly to wild-type levels, confirming that *HOP1* is dominant regarding spore formation and spore viability. In comparison, the spore viability of the *hop1*Δ*/hop1CTD* strain decreased to undetectable levels, indicating that the Hop1CTD was unable to complement the spore viability defect of *hop1*Δ strain. Nevertheless, taken together, these data suggest that Hop1CTD although localizes to the nucleus and is functionally equivalent to the full-length Hop1 in terms of its *in vitro* activities it is unable to complement the meiotic recombination defects of *hop1*Δ strain.

## DISCUSSION

In this study, we show that *S. cerevisiae* Hop1 has a modular domain organization, consisting of an intrinsically disordered N-terminus and a protease-resistant C-terminal domain. Additional evidence revealed that the 35 kDa C-terminal domain exhibits strong homotypic and heterotypic protein–protein interactions, and its biochemical activities were similar to those of full-length Hop1. However, Hop1CTD failed to complement the meiotic recombination defects of *hop1* null strain.

**Modular Domain Architecture of Hop1.** So far all our attempts to crystallize full-length Hop1 failed; therefore, we performed limited proteolysis to identify functional domains. These studies revealed that full-length Hop1 contains three distinct domains encompassing residues 1–268 (N-terminus), 269–605 (Hop1CTD), and 560–605 (short C-terminal tail) (Figure 2G). The existence of protease-sensitive N-terminus and extreme C-terminal tail indicates that these are exposed flexible domains, each of these connecting independently to the folded central globular domain. Indeed, many proteins have evolved modular architectures with distinct domains that are able to act independently or cooperatively to perform a common task. For example, separate structural domains often provide multiple binding sites that increase the affinity for one ligand or that enable the protein to contact multiple ligands in a concerted or sequential fashion.[38] In addition, it is possible that the presence of disordered N-terminus may be advantageous because it allows Hop1 to partner with other structural components of SC. Genetic and *in vitro* evidence suggests that Red1 and Hop1 proteins physically interact with each other and


dx.doi.org/10.1021/bi4005528 | *Biochemistry* 2013, 52, 5265–5279

affect the same subset of meiotic recombination events, indicating that they function through a common pathway.[15,22,39] Thus, it is conceivable that the disordered N-terminal domain might facilitate interaction between Hop1 and Red1, and possibly with other SC proteins.

**Functional Analysis of Hop1 Protein.** An incisive genetic study of *HOP1* has established that its gene product functions within a multimeric complex.[22] Our studies show that Hop1 N-terminus truncation did not have a major impact on its function *in vitro*. Like full-length Hop1, different approaches revealed that Hop1CTD forms multiple oligomeric species. Using EMSA, we show that Hop1CTD binds HJ and G4DNA with sub-nanomolar affinity. Our data also show that Hop1CTD was able to promote intra- and intermolecular synapsis between DNA molecules. Fluorescence studies highlighted several points of divergence between these proteins. One was the ability of full-length Hop1 to quench ANS fluorescence but not by Hop1CTD. A second variance was the finding that Hop1CTD was extremely resistant to proteolytic degradation, consistent with the notion that it is likely to be the "core" domain of Hop1 protein. Finally, we found that Hop1CTD appears to be less efficient in DNA bridging, compared to full-length Hop1. Perhaps one of the most unexpected and novel findings of our analysis was the observation that Hop1CTD, although it localizes to the nucleus in the *hop1*Δ mutant, failed to complement the meiotic recombination defects of the *hop1*Δ strain.

**Structural Components of SC Lateral Elements.** Biochemical characterization of the full complement of SC proteins and the functional significance of these proteins remains an important area of investigation. Although a number of structural components of SC have been identified in different organisms,[2−4] seven different LE proteins are known: SYCP2 and SYCP3 in mice,[40,41] Hop1 and Red1 in *S. cerevisiae* and *Kluyveromyces lactis*,[14,16,17] *ORD* in *Drosophila melanogaster*,[42] *PAIR3* in *Oryza sativa*,[43] *HTP-3* and *HIM-3* in *Caenorhabditis elegans*,[44−46] In *S. cerevisiae*, the SC components include Hop1, Red1, Zip1, Zip2, Zip3, Zip4, and Mek1.[13,14,16,18,19,47,48] Among these, *HOP1* and *RED1* encode structural components of LE, which colocalize to the axial cores of meiotic chromosomes, and are required for homologous chromosome synapsis and chiasma formation.[11,14,16,19,21,25] Consistent with this idea, genetic evidence suggests that homologue alignment is impaired in *red1hop1* strains and/or that the associations between homologues are less stable than in wild type.[38,49] *red1* mutants fail to make any discernible AE or SC structures and exhibit normal chromosome condensation, while *hop1* mutants form long fragments of AEs but without any SCs, are defective in chromosome condensation, and produce no viable spores.[16,23,36,48,49] In both *S. cerevisiae* and *S. pombe*, Mek1, a protein kinase, functions together with Red1 and Hop1 to ensure interhomologue recombination and establishes a barrier to the use of a sister chromatid as the template.[16,19,50]

The functional homologues of *S. cerevisiae* Hop1 exist across species, indicating that *HOP1* function is conserved throughout evolution. However, *K. lactis HOP1* complements *S. cerevisiae hop1* mutant poorly, perhaps due to species-specific variations.[17] In *Arabidopsis thaliana* and *Brassica*, Hop1 homologue is *ASY1*, which localizes to the meiotic chromosome axis.[51,52] In the absence of *ASY1*, the synapsis is interrupted and chiasma formation is dramatically reduced.[51−53] In *C. elegans*, *HIM-3* and *HTP-3* are essential for homologue pairing, synapsis and crossing over, and acts as a barrier-to-sister chromatid exchange during recombination.[54] In mice, SYCP2 and SYCP3 are the only two known structural components of LEs.[39,55,56] Mutant mice lacking SYCP2 and SYCP3 exhibit defects in the integrity of meiotic chromosomes, SC assembly, and meiotic recombination.[40,41]

**Synapsis of Homologous Chromosomes During Meiosis.** The mechanism by which each chromosome finds its homologous partner, recombines with it, and eventually segregates into each gamete is the core event in meiosis.[57−59] Although many details of the mechanistic aspects that underlie DNA strand exchange have been uncovered, the mechanistic basis of chromosome synapsis has remained a mystery since B. McClintock[60] first noted the fundamental problem of homology recognition and synapsis. Moreover, far less is known about the chromosome configurations during meiosis.[1−4,61]

In many eukaryotes, two hallmark characteristics of meiotic prophase are the cytologically visible manifestation of SC and high levels of homologous recombination.[5,6] Although the components of SC are thought to play a central role in synapsis of homologues, one outstanding question not answered to date is whether or how SC-related proteins catalyze interaction between homologues. In *S. cerevisiae*, mice, *Sordaria macrospora* and *Zea mays*, real time physical assays and/or genetic analyses show that recombination occurs prior to the manifestation of cytologically visible SC, as deduced from chromosomal localization of recombination-associated proteins.[6] On the other hand, in *C. elegans* the juxtaposition of homologue axes and the assembly of SC precede events associated with reciprocal recombination.[45] Thus, while it is conceivable that subtle functional differences do exist and may emerge following further analysis, current data strongly suggest multiple mechanisms including *SPO11*-independent pathways to chromosome pairing contribute to the recognition and stable pairing of homologues during meiosis.[1,2,6,8,62] The basis for these interspecies differences remains to be determined, but clearly, comparisons among organisms will continue to be informative for defining the interplay between reciprocal recombination and synapsis. In summary, the structure−function studies of Hop1 begun here provide a framework that will further elucidate the molecular mechanisms of interaction between components of the SC and help develop assays for studies on SC-related proteins.

## ■ ASSOCIATED CONTENT

### Ⓢ Supporting Information

Sequences of oligonucleotides used in this study (Table S1), list of plasmid constructs used in this study (Table S2), time-dependent spontaneous digestion of full-length Hop1 protein (Figure S1), Hop1CTD cross-linking with DIDS (Figure S2), and width measurements (Figure S3). This material is available free of charge via the Internet at http://pubs.acs.org.

## ■ AUTHOR INFORMATION

### Corresponding Author

*Tel.: +91 80 2293 2235/2360 0278; fax: +91 80 2360 0814/0683; e-mail: kmbc@biochem.iisc.ernet.in.

### Funding

This work was supported by a grant (SR/SO/BB-94/2010) and J. C. Bose National Fellowship from the Department of Science and Technology, Government of India, New Delhi, to K.M.

### Notes

The authors declare no competing financial interest.
[§]Deceased.

## ■ ACKNOWLEDGMENTS

We gratefully acknowledge S. Usha and N. S. Srilatha for their expert technical assistance with AFM and SPR measurements, respectively.

## ■ ABBREVIATIONS

AE, axial elements; AFM, atomic force microscope; bp, base pairs; ANS, 1-anilino-8-naphthalene sulfonate; DLS, dynamic light scattering; DSB, double-stranded DNA break; dsDNA, double-stranded DNA; DTT, dithiothreitol; EDTA, ethylene diamine tetraacetic acid; EMSA, electrophoretic mobility shift assay; HJ, Holliday junction; LE, lateral elements; ODNs, oligonucleotides; PAGE, polyacrylamide gel electrophoresis; SC, synaptonemal complex; SDS, sodium dodecyl sulfate; ssDNA, single-stranded DNA; SPR, surface plasmon resonance

## ■ REFERENCES

(1) Zickler, D., and Kleckner, N. (1999) Meiotic chromosomes: integrating structure and function. *Annu. Rev. Genet. 33*, 603−754.
(2) Zickler, D. (2006) From early homologue recognition to synaptonemal complex formation. *Chromosoma 115*, 158−174.
(3) Roeder, G. S. (1997) Meiotic chromosomes: it takes two to tango. *Genes Dev. 11*, 2600−2621.
(4) Anuradha, S., and Muniyappa, K. (2005) Molecular aspects of meiotic chromosome synapsis and recombination. *Prog. Nucl. Acids Res. Mol. Biol. 79*, 49−132.
(5) Barzel, A., and Kupiec, M. (2008) Finding a match: how do homologous sequences get together for recombination? *Nat. Rev. Genet. 9*, 27−37.
(6) Page, S. L., and Hawley, R. S. (2004) The genetics and molecular biology of the synaptonemal complex. *Annu. Rev. Cell Dev. Biol. 20*, 525−558.
(7) Paques, F., and Haber, J. E. (1999) Multiple pathways of recombination induced by double-strand breaks in *Saccharomyces cerevisiae*. *Microbiol. Mol. Biol. Rev. 63*, 349−404.
(8) Burgess, S. M. (2002) Homologous chromosome associations and nuclear organization in the budding yeast, *Saccharomyces cerevisiae*, in *Homology Effects. Adv. Genet.* Vol. *46*, pp 49−90, Academic Press, San Diego.
(9) Heyer, W. D., Ehmsen, K. T., and Liu, J. (2010) Regulation of homologous recombination in eukaryotes. *Annu. Rev. Genet. 44*, 113−139.
(10) Allers, T., and Lichten, M. (2001) Differential timing and control of non-crossover and crossover recombination during meiosis. *Cell 106*, 47−57.
(11) Fung, J. C., Rockmill, B., Odell, M., and Roeder, G. S. (2004) Imposition of crossover interference through the nonrandom distribution of synapsis initiation complexes. *Cell 116*, 795−802.
(12) Peoples-Holst, T. L., and Burgess, S. M. (2005) Multiple branches of the meiotic recombination pathway contribute independently to homolog pairing and stable juxtaposition during meiosis in budding yeast. *Genes Dev. 19*, 863−874.
(13) Agarwal, S., and Roeder, G. S. (2000) Zip3 provides a link between recombination enzymes and synaptonemal complex proteins. *Cell 102*, 245−255.
(14) Hollingsworth, N. M., Goetsch, L., and Byers, B. (1990) The *HOP1* gene encodes a meiosis-specific component of yeast chromosomes. *Cell 61*, 73−84.
(15) Hollingsworth, N. M., and Johnson, A. D. (1993) A conditional allele of the yeast *HOP1* gene is suppressed by overexpression of two other meiosis-specific genes: *RED1* and *REC104*. *Genetics 133*, 785−797.
(16) Smith, A. V., and Roeder, G. S. (1997) The yeast Red1 protein localizes to the cores of meiotic chromosomes. *J. Cell Biol. 136*, 957−967.
(17) Smith, A. V., and Roeder, G. S. (2000) Cloning and characterization of the Kluyveromyces lactis homologs of the *Saccharomyces cerevisiae RED1* and *HOP1* genes. *Chromosoma 109*, 50−61.
(18) Sym, M., Engebrecht, J., and Roeder, G. S. (1993) *ZIP1* is a synaptonemal complex protein required for meiotic chromosome synapsis. *Cell 72*, 365−378.
(19) Bailis, J. M., and Roeder, G. S. (2000) Pachytene exit controlled by reversal of Mek1-dependent phosphorylation. *Cell 101*, 211−221.
(20) Blat, Y., Protacio, R. U., Hunter, N., and Kleckner, N. (2002) Physical and functional interactions among basic chromosome organizational features govern early steps of meiotic chiasma formation. *Cell 111*, 791−802.
(21) de los Santos, T., and Hollingsworth, N. M. (1999) Red1p: a *MEK1*-dependent phosphoprotein that physically interacts with Hop1p during meiosis in yeast. *J. Biol. Chem. 274*, 1783−1790.
(22) Friedman, D. B., Hollingsworth, N. M., and Byers, B. (1994) Insertional mutations in the yeast *HOP1* gene: Evidence for multimeric assembly in meiosis. *Genetics 136*, 449−464.
(23) Loidl, J., Klein, F., and Scherthan, H. (1994) Homologous pairing is reduced but not abolished in asynaptic mutants of yeast. *J. Cell Biol. 125*, 1191−1200.
(24) Woltering, D., Baumgartner, B., Bagchi, S., Larkin, B., Loidl, J., de los Santos, T., and Hollingsworth, N. M. (2000) Meiotic segregation, synapsis, and recombination checkpoint functions require physical interaction between the chromosomal proteins Red1p and Hop1p. *Mol. Cell. Biol. 20*, 6646−6658.
(25) Borner, G. V., Kleckner, N., and Hunter, N. (2004) Crossover/noncrossover, differentiation, synaptonemal complex formation, and regulatory surveillance at the leptotene/zygotene transition of meiosis. *Cell 117*, 29−45.
(26) Klein, F., Mahr, P., Galova, M., Buonomo, S. B., Michaelis, C., Nairz, K., and Nasmyth, K. (1999) A central role for cohesins in sister chromatid cohesion, formation of axial elements, and recombination during yeast meiosis. *Cell 98*, 91−103.
(27) Anuradha, S., and Muniyappa, K. (2004) Saccharomyces cerevisiae Hop1 zinc finger motif is the minimal region required for its function *in vitro*. *J. Biol. Chem. 279*, 28961−28969.
(28) Anuradha, S., and Muniyappa, K. (2004) Meiosis-specific yeast Hop1 protein promotes synapsis of double-stranded DNA helices via the formation of guanine quartets. *Nucleic Acids Res. 32*, 2378−2385.
(29) Kironmai, K. M., Muniyappa, K., Friedman, D., Hollingsworth, N. M., and Byers, B. (1998) DNA-binding activities of Hop1 protein, a synaptonemal complexcomponent from *Saccharomyces cerevisiae*. *Mol. Cell. Biol. 18*, 1424−1435.
(30) Muniyappa, K., Anuradha, S., and Byers, B. (2000) Yeast meiosis-specific protein Hop1 binds to G4-DNA and promotes its formation. *Mol. Cell. Biol. 20*, 1361−1369.
(31) Tripathi, P., Anuradha, S., Ghosal, G., and Muniyappa, K. (2006) Selective binding of meiosis-specific yeast Hop1 protein to the Holliday junctions distorts the DNA structure and its implications for junction migration and resolution. *J. Mol. Biol. 364*, 599−611.
(32) Khan, K., Karthikeyan, U., Li, Y., Yan, J., and Muniyappa, K. (2012) Single-molecule DNA analysis reveals that yeast Hop1 protein promotes DNA folding and synapsis: Implications for condensation of meiotic chromosomes. *ACS Nano 6*, 10658−10666.
(33) Mumberg, D., Mailer, R., and Funk, M. (1995) Yeast vectors for the controlled expression of heterologous proteins in different genetic backgrounds. *Gene 156*, 119−122.
(34) Khan, K., Madhavan, T. P. V., and Muniyappa, K. (2010) Cloning, overexpression and purification of functionally active Saccharomyces cerevisiae Hop1 protein from *Escherichia coli*. *Protein Expr. Purif. 72*, 42−47.
(35) Hennessey, J. P., and Johnson, W. C., Jr. (1981) Information content in the circular dichroism of proteins. *Biochemistry 20*, 1085−1094.

(36) Yamamoto, T., Iino, H., Kim, K., Kuramitsu, S., and Fukui, K. (2011) Evidence for the ATP-dependent structural rearrangement of the nuclease catalytic site in the DNA mismatch repair endonuclease MutL. *J. Biol. Chem. 286*, 42337−42348.
(37) Hawe, A., Sutter, M., and Jiskoot, W. (2006) Extrinsic fluorescent dyes as tools for protein characterization. *Pharm. Res. 25*, 1487−1499.
(38) Moore, A. D., Björklund, A. K., Ekman, D., Bornberg-Bauer, E., and Elofsson, A. (2008) Arrangements in the modular evolution of proteins. *Trends Biochem. Sci. 3*, 444−451.
(39) Rockmill, B., and Roeder, G. S. (1990) Meiosis in asynaptic yeast. *Genetics 126*, 563−574.
(40) Yang, F., De La Fuente, R., Leu, N. A., Baumann, C., McLaughlin, K. J., and Wang, P. J. (2006) Mouse *SYCP2* is required for synaptonemal complex assembly and chromosomal synapsis during male meiosis. *J. Cell Biol. 173*, 497−507.
(41) Yuan, L., Liu, J. G., Zhao, J., Brundell, E., Daneholt, B., and Hoog, C. (2000) The murine *SCP3* gene is required for synaptonemal complex assembly, chromosome synapsis, and male fertility. *Mol. Cell 5*, 73−83.
(42) Webber, H. A., Howard, L., and Bickel, S. E. (2004) The cohesion protein *ORD* is required for homologue bias during meiotic recombination. *J. Cell Biol. 164*, 819−829.
(43) Wang, K., Wang, M., Tang, D., Shen, Y., Qin, B., et al. (2011) *PAIR3*, an axis associated protein, is essential for the recruitment of recombination elements onto meiotic chromosomes in rice. *Mol. Biol. Cell 22*, 12−19.
(44) Couteau, F., and Zetka, M. (2005) *HTP-1* coordinates synaptonemal complex assembly with homolog alignment during meiosis in *C. elegans*. *Genes Dev. 19*, 12744−2756.
(45) Couteau, F., Goodyer, W., and Zetka, M. (2004) Finding and keeping your partner during meiosis. *Cell Cycle 3*, 1014−1016.
(46) Zetka, M. C., Kawasaki, I., Strome, S., and Muller, F. (1999) Synapsis and chiasma formation require HIM-3, a meiotic.chromosome core component that functions in chromosome segregation in *Caenorhabditis elegans*. *Genes Dev. 13*, 2258−2270.
(47) Chua, P. R., and Roeder, G. S. (1998) Zip2, a meiosis-specific protein required for the initiation of chromosome synapsis. *Cell 93*, 349−59.
(48) Tsubouchi, T., Zhao, H., and Roeder, G. S. (2006) The meiosis-specific zip4 protein regulates crossover distribution by promoting synaptonemal complex formation together with zip2. *Dev. Cell. 10*, 809−819.
(49) Hollingsworth, N. M., and Byers, B. (1989) *HOP1*: a yeast meiotic pairing gene. *Genetics 121*, 445−462.
(50) Latypov, V., Rothenberg, M., Lorenz, A., Octobre, G., Csutak, O., Lehmann, E., Loidl, J., and Kohli, J. (2010) Roles of Hop1 and Mek1 in meiotic chromosome pairing and recombination partner choice in *Schizosaccharomyces pombe*. *Mol. Cell. Biol. 30*, 1570−1581.
(51) Armstrong, S. J., Caryl, A. P., Jones, G. H., and Franklin, F. C. (2002) Asy1, a protein required for meiotic chromosome synapsis, localizes to axis-associated chromatin in *Arabidopsis and Brassica*. *J. Cell Sci. 115*, 3645−3655.
(52) Caryl, A. P., Armstrong, S. J., Jones, G. H., and Franklin, F. C. (2000) A homologue of the yeast *HOP1* gene is inactivated in the Arabidopsis meiotic mutant *asy1*. *Chromosoma 109*, 62−71.
(53) Golubovskaya, I. N., Wang, C. J., Timofejeva, L., and Cande, W. Z. (2011) Maize meiotic mutants with improper or non-homologous synapsis due to problems in pairing or synaptonemal complex formation. *J. Exp. Bot. 26*, 1533−1544.
(54) Severson, A. F., Ling, L., van Zuylen, V., and Meyer, B. J. (2009) The axial element protein HTP-3 promotes cohesin loading and meiotic axis assembly in *C. elegans* to implement the meiotic program of chromosome segregation. *Genes Dev. 23*, 1763−1778.
(55) Offenberg, H. H., Schalk, J. A., Meuwissen, R. L., van Aalderen, M., Kester, H. A., Dietrich, A. J., and Heyting, C. (1998) *SCP2*: a major protein component of the axial elements of synaptonemal complexes of the rat. *Nucleic Acids Res. 26*, 2572−2579.
(56) Pelttari, J., Hoja, M. R., Yuan, L., Liu, J. G., Brundell, E., Moens, P., Santucci-Darmanin, S., et al. (2001) A meiotic chromosomal core consisting of cohesin complex proteins recruits DNA recombination proteins and promotes synapsis in the absence of an axial element in mammalian meiotic cells. *Mol. Cell. Biol. 21*, 5667−5677.
(57) Kleckner, N., and Weiner, B. M. (1993) Potential advantages of unstable interactions for pairing of chromosomes in meiotic, somatic, and premeiotic cells. *Cold Spring Harbor Symp. Quant. Biol. 58*, 553−565.
(58) Schwacha, A., and Kleckner, N. (1994) Identification of joint molecules that form frequently between homologs but rarely between sister chromatids during yeast meiosis. *Cell 76*, 51−63.
(59) Nag, D. K., Scherthan, H., Rockmill, B., Bhargava, J., and Roeder, G. S. (1995) Heteroduplex DNA formation and homolog pairing in yeast meiotic mutants. *Genetics 141*, 75−86.
(60) McClintock, B. (1933) The association of non-homologous parts of chromosomes in the mid-prophase of meiosis in *Zea mays*. *Z. Zellforsch. Microsk. Anat. 19*, 191−237.
(61) Maguire, M. P. (1984) The mechanism of meiotic homologue pairing. *J. Theor. Biol. 106*, 605−615.
(62) Panizza, S., Mendoza, M. A., Berlinger, M., Huang, L., Nicolas, A., Shirahige, K., and Klein, F. (2011) Spo11-accessory proteins link double-strand break sites to the chromosome axis in early meiotic recombination. *Cell 146*, 372−383.